People Detection using Range and Intensity Data from Multi-Layered Laser Range Finders

Alexander Carballo, Akihisa Ohya and Shin'ichi Yuta

Abstract— Effective detection of people is a basic require-
ment for robot coexistence in human environments. In our
previous work [1] we proposed a method for people detection
and position estimation using multiple layers of Laser Range
Finders (LRF) in a mobile robot. We extend our work by
introducing laser reflection intensity as a novel feature for
people detection, achieving significant improvement of detection
rates. In concrete, we propose a method for calibration of laser
intensity data, a method for segment separation using laser
intensity, and introduce two new intensity-based features for
people detection: the variance of laser intensity and the variance
of intensity differences. We present experimental results that
confirm the effectiveness of our multi-layered detection method
including laser intensity.

I. INTRODUCTION

Laser Range Finders (LRF) are an important part of people
detection and tracking systems in surveillance and robot and
human interaction systems. LRFs present important advan-
tages like high accuracy, wide view angles, fast scanning
rates, etc., and are becoming more accessible and safe for
usage in human environments. Due to safety regulations,
applications using non class-1 lasers are mostly limited to
low positions. Thus legs have been widely used for human
detection and tracking [2–5]. Using LRFs in a multi-layered
arrangement to detect other complementary features (waist,
chest, head, etc.) has been proposed recently [1, 6, 7].

Supervised learning using the AdaBoost algorithm
(Schapire *et al.* [8]) has proven very successful for correct
detection people features from LRF segments [5, 7, 9]: using
a set of geometrical features from LRF range data (e.g.,
width, linearity, curvature, etc.), define weak classifiers and
then train a strong classifier.

When compared to other sensors (e.g., vision), a limitation
of LRFs is that range data is not enough to distinguish
physically different objects when they are in contact (e.g., a
person leaning against a wall), LRF scan points get combined
into one big segment even if a very small jump distance
is used. Existing solutions include adding time dimension
to LRF segments and measure segment motion between
consecutive scans [5], keeping tracks for each target [10–
12], or else using normal vectors and 3D LRF [13].

In [1] we introduced a multi-layered people detection
system for a people group companion robot. Four LRF
sensors are installed in a mobile robot, arranged in pairs
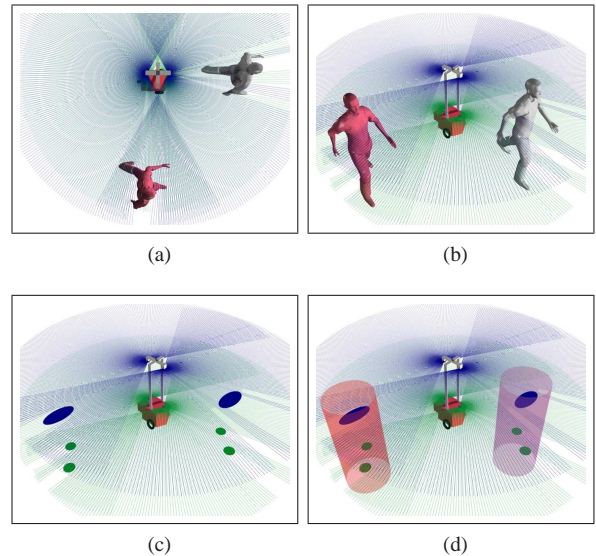in two layers (Fig. 1(a) and Fig. 1(b)), and data from each

Intelligent Robot Laboratory, Graduate School of Systems and
Information Engineering, University of Tsukuba, 1-1-1 Tennoudai,
Tsukuba City Ibaraki Pref., 305-8573, Japan, +81-29-853-6168.
{acs,ohya,yuta}@roboken.esys.tsukuba.ac.jp

Fig. 1: Multi-layered people detection: (a) two sensors per
layer (bird's-eye view); (b) two layers of sensors; (c) detec-
tion of body parts in each layer, and (d) people detection.

independent layer is processed in parallel. Scan data is first
divided into segments, for each segment we compute a set
of features for classification of body parts from each person
around the robot (legs in the bottom layer and chests in the
top layer, Fig. 1(c)). Finally detected parts are fused to detect
people and their position (Fig. 1(d)). Our system is tolerant
to occlusions by keeping an association of current scan data
with the position of previously detected people.

We extend further our work by introducing laser reflec-
tion intensity as a novel feature for people detection and
for segment separation. To our knowledge no other work
considers laser reflection intensity for people detection. The
contributions of this work can be summarized as follows:

- Introduction of laser reflection intensity as a new feature
  for people detection
- A method for separation of segments using laser reflec-
  tion intensity
- A simple technique for calibration of laser reflection
  intensity for low power LRFs

The rest of the paper is as follows: Section II briefly
describes our people detection system. In Section III we
explain and propose laser reflection intensity as a new tool
for people detection. Section IV presents experimental results
of our people detection method and finally, conclusions and
future works are left for Section V.

II. System Overview

For each layer, sensors facing opposite directions (see Fig. 1a) are fused [1] to produce a 360° representation of robot's surroundings. Fused data is divided into segments using an adaptive threshold [1] to find breakpoints (jump distance). For every segment S_i we compute a set of n features $\mathbf{h}(S_i) \in \mathbb{R}^n$ to judge whether the segment corresponds to body part (chest or leg). Based on Arras *et al.* [5], we defined the following list of features from every segment:

1) **Number of points** (N) of the segment.
2) **Width** (w), longest side of the segment's bounding box $w = \max(W, H)$, with W and H the sides of the box.
3) **Size ratio** (ℓ), ratio of the sides of the segment's bounding box $\ell = \frac{\max(W,H)}{\min(W,H)}$.
4) **Linearity** (L) variance of residuals of best fitting line.
5) **Circularity** (c) variance of residuals of best fit circle.
6) **Radius** (R), from the best fitting circle.
7) **Ellipticity** (ε), variance of residuals of best fit ellipse.
8) **Boundary length** (bl), average distance between points $bl = \frac{1}{N} \sum_{i=1}^{N-1} D(f_i, f_{i+1})$.
9) **Boundary regularity** (br): standard deviation of the boundary length.
10) **Mean curvature** ($\bar{\kappa}$): mean of the curvatures κ_i from the triangle $\triangle f_{i-1}f_i f_{i+1}$, every three points, $\kappa_i = \frac{4A}{D(f_{i-i},f_i)D(f_i,f_{i+1})D(f_{i-1},f_{i+1})}$, A triangle's area.
11) **Mean angular difference** ($\bar{\phi}$): mean of the angles ϕ_i every three points as $\phi_i = \measuredangle(\overline{f_{i-1}f_i}, \overline{f_i f_{i+1}})$.
12) **Normalized number of points** ($\hat{N}$), the ratio of the actual number of points and the maximum expected number of points at a given range, $\hat{N} = \frac{2N\rho \tan(\vartheta/2)}{w_{\max}}$, where ρ is the range to the segment center, ϑ is the angular resolution of the sensor and $w_{\max}$ is the maximum expected width of a person.

Following the description in Arras *et al.* [5], we use the generalized AdaBoost algorithm to train a strong classifier $\mathcal{H}$ to classify body parts. For that we define a set of m labeled training examples $\mathcal{X} = \langle(\mathbf{h}(S_1), l_1), \ldots, (\mathbf{h}(S_m), l_m)\rangle$ with $l_i \in \{+1, -1\}$ the segment's label where $l_i = +1$ is for positive examples (a person) and $l_i = -1$ for negative examples (an environment object). Following Martínez Mozos *et al.* [7], to define labels of $\mathcal{X}$ we set an obstacle free area around the robot, any segment which enters this area is automatically labeled as $+1$ and the rest as -1. The final strong classifier $\mathcal{H}$ is:

$$\mathcal{H}(S) = \text{sign}\left(\sum_{t=1}^{T} \omega_t g_t(S)\right) \quad (1)$$

The weak classifier function $g_t(S)$ evaluates the t-th feature $h_t(S)$ as follows:

$$g_t(S) = \begin{cases} +1 & \text{if } s_t h_t(S) < s_t \theta_t, \\ -1 & \text{otherwise.} \end{cases} \quad (2)$$

AdaBoost learns the parameters: ω_t which is a weight applied to the weak classifier g_t, θ_t the threshold for the feature h_t and $s_t \in \{+1, -1\}$ the sign defining the direction of the inequality. The number of weak classifiers T that form the final strong classifier was defined as $T = 100$ which allows

good performance and small classification errors. We trained two separated strong classifiers, $\mathcal{H}_{\text{top}}$ to detect chest segments in the top layer and $\mathcal{H}_{\text{bottom}}$ to detect legs in the bottom layer (see Fig. 1c). Finally we label segments as *candidate* using the output from both $\mathcal{H}_{\text{top}}$ and $\mathcal{H}_{\text{bottom}}$.
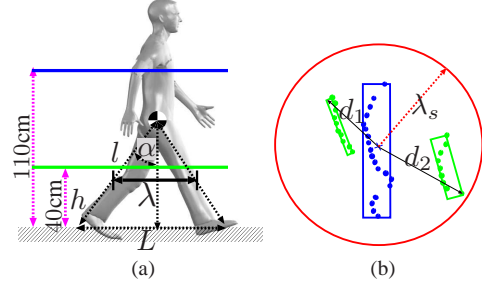

Fig. 2: Walking model and layer fusion: (a) separation between legs λ at sensor height h, and (b) search area for association.

To combine candidate segments from both layers (see Fig. 2(a)), we define a search radius of $\lambda_s = \frac{\lambda}{2} + \xi$, according to the separation between legs $\lambda = 2(L\cos(\alpha) - h)\tan(\alpha)$ [1] and for some bias ξ. The chest segment is projected into the bottom layer (bird's-eye view in Fig. 2(b)) to search for the corresponding leg(s). If the distance from the chest center to the furthest leg segment point (d_1 and d_2 in Fig. 2(b)) is less than λ_s we successfully detect a person. We set $\lambda = 35.42cm$ for normal walking speed and $\xi = 12cm$.

For every person $\mathcal{P}_i$ the center of the chest ellipse is used as the expected position $\mu_i = \begin{bmatrix} x_i & y_i \end{bmatrix}^{\mathsf{T}}$ of the person and the radius λ_s to define the initial covariance matrix of the actual position $\Sigma_i = \lambda_s \boldsymbol{I}$. Every newly detected person $\widehat{\mathcal{P}}_i^t$ in time t is associated with a known person $\mathcal{P}_k^{t-1}$ from a list $\mathcal{P}^{t-1}$ from time $t-1$. To achieve this association, for every new person $\widehat{\mathcal{P}}_i^t$ we find the closest $\mathcal{P}_k^{t-1}$ using the Mahalanobis distance $d(i, k)$ with the estimated positions (μ_i^t, Σ_i^t) for $\widehat{\mathcal{P}}_i^t$ and $(\mu_k^{t-1}, \Sigma_k^{t-1})$ for $\mathcal{P}_k^{t-1}$. If the minimum $d(i, k)$ is smaller than some d_{max} then $\widehat{\mathcal{P}}_i^t$ and $\mathcal{P}_k^{t-1}$ are associated in the new list $\mathcal{P}^t$, else $\widehat{\mathcal{P}}_i^t$ is regarded as a new person included $\mathcal{P}^t$.

Tolerance to occlusions is achieved by relaxing this data association to allow single body parts, this is candidate segments for which no corresponding part could be found in the opposite layer, to become associated to known persons (partial association). In the current implementation we tested only partial association for chest segments since occlusions are much more common in the bottom layer.

III. Laser Intensity for People Detection

Most LRF sensors provide reflection intensity data for every laser beam. This property has been rarely used, one pioneer work using laser intensity from a vehicle is attributed to Hancock [14], physical models of laser reflection of their sensor were proposed according to the differences in surface albedo, roughness, range to target, etc.; with different calibration models, according to the type of surface to scan from the vehicle (e.g., asphalt), they were able to extract clear

intensity images. Recently laser intensity is gaining interest: Nüchter *et al.* [15, 16] uses range and intensity data together with Haar-like features for object classification. In Montemerlo *et al.* [17] laser intensity is used for extracting road lanes from an autonomous vehicle, based on the reflection difference of asphalt and road lanes.

Different from related works [14–17], where high-power laser sensors for long ranges are used (the Z+F laser for ranges up to 400m, the SICK *LMS 200* and *LMS 291-S14* up to 80m, and the RIEGL *LMS-Q120* up to 150m), instead we use low-power laser scanners: the Hokuyo *URG-04LX* range scanner, with a maximum range of 5.6m. The intensity value in the *URG-04LX* decays very quickly with range (Kawata *et al.* [18]), so same object will show different laser intensity values in rather short ranges; therefore we require to calibrate the laser intensity response before using it.

According to [18], the reflected laser arrives at the sensor's photo-diode with low power and it is processed through filters, correction tables and amplifiers in the sensor's circuitry. For any laser beam, if the amplified laser intensity is over some internal threshold, the sensor will report the range data for that beam otherwise it is regarded as out-of-range in the sensor output. In consequence, the physical laser intensity and the sensor's intensity output are not linearly related, existing models of LRF intensity cannot be used.

A. Calibration of Laser Intensity

The *URG-04LX* presents a characteristic *sigmoid* curve for intensity decay with range. Based on the *Gompertz* growth function[19], we defined the decay function for intensity as a function of range as:

$$\mathcal{F}_\rho(i) = a\left(1 - \exp(b\exp\left(c\rho_i\right))\right) \qquad (3)$$

where ρ is the i-th beam's range, a is the upper asymptote, b and c (both negative numbers) are decay parameters. Nonlinear least squares was used to find the parameters (a, b, c). This characteristic sigmoid form can be clearly appreciated in
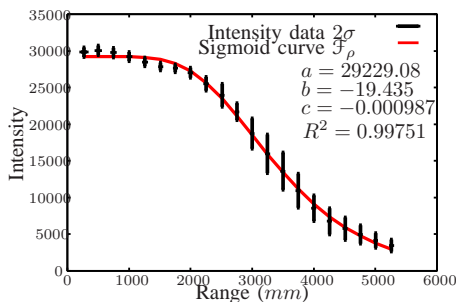

Fig. 3: Characteristic intensity data by varying distance and sigmoid curve for the URG-04LX sensor.

Fig. 3. This curve was obtained from a white target ($90g/m^2$, $0.13mm$ white bond paper) with an angle of incidence close to zero (vertical error bars for two standard deviations 2σ, data was collected during $60s$ at each range), the continuous curve corresponds to the function $\mathcal{F}_\rho$ fitted to white paper data with the given parameters.

Using Eq. 3 as the maximum expected intensity, we normalize (calibrate) the actual intensity value I_i of the i-th scan point p_i as:

$$\mathcal{I}(p_i) = \frac{I_i}{\mathcal{F}_\rho(p_i)} \qquad (4)$$

B. Laser Intensity and People Detection

When two objects stand very close their range-based segments get combined and cannot be detected individually. From laser reflection, one object resulting from combining two or more objects with different reflection properties will have a larger variance of intensity values $\sigma_\mathcal{J}^2$ resulting from mixing the intensities of the individual objects. Furthermore, if we consider how intensity changes between consecutive points p_i^j and p_{i+1}^j in a segment j using the difference $\mathcal{D}_j(i) = \mathcal{I}(p_i^j) - \mathcal{I}(p_{i+1}^j)$, we can define the *intensity uniformity* of an object by the *variance of intensity differences* $\sigma_\mathcal{D}^2$: if the object has uniform reflection (i.e., a smooth surface with a single color) then $\sigma_\mathcal{D}^2$ will be small as the differences tend to be small. The *variance of intensity differences* between points on a segment j is:

$$\sigma_{\mathcal{D}_j}^2 = \frac{1}{N}\sum_{i=1}^{N}\left(\mathcal{D}_j(i) - \mu_{\mathcal{D}_j}\right)^2 \qquad (5)$$

where $\mu_{\mathcal{D}_j}$ is the average of such difference over all the points in segment j. After analyzing intensity data from people and environment objects, we found that the variance $\sigma_\mathcal{D}^2$ is large for all the segments from people, even cases of a person very close to another object (merged). This large variance $\sigma_\mathcal{D}^2$ usually comes from large values of the variance of calibrated intensity $\sigma_\mathcal{J}^2$ which provides a measurement the variations of intensity (i.e diffuse reflection) of an object. Therefore, we extended the list in Section II with the following new features for people detection:

13) **Intensity variation** ($\sigma_\mathcal{J}^2$), the variance of calibrated intensity.
14) **Intensity uniformity** ($\sigma_\mathcal{D}^2$), the variance of differences of calibrated intensity as in Eq. 5.

Using AdaBoost we train two new strong classifiers $\mathcal{H}_{\text{top}}^+$ and $\mathcal{H}_{\text{bottom}}^+$ (one per layer) including these new intensity-based features.

We are interested in detecting people even when their LRF segments are merged with other objects. To detect such person-merged segments using only range information, an intuitive method will be to look for wide segments (more than some maximum width $w_{\max}$) that are not straight lines like walls (a size ratio ℓ under some $\ell_{\max}$); however several large and irregular objects like corners, book shelves, etc., conform to that test. To improve the merged segment detection test, we can use additionally intensity information and look for segments with large $\sigma_\mathcal{D}^2$ (variance $\sigma_\mathcal{D}^2$ over some $\sigma_{\mathcal{D}_{min}}^2$). The values $w_{\max}$ and $\ell_{\max}$ are defined as the maximum thresholds θ_w and θ_ℓ learned for the strong classifier $\mathcal{H}_{\text{top}}$, $\sigma_{\mathcal{D}_{min}}^2$ from the classifier $\mathcal{H}_{\text{top}}^+$.

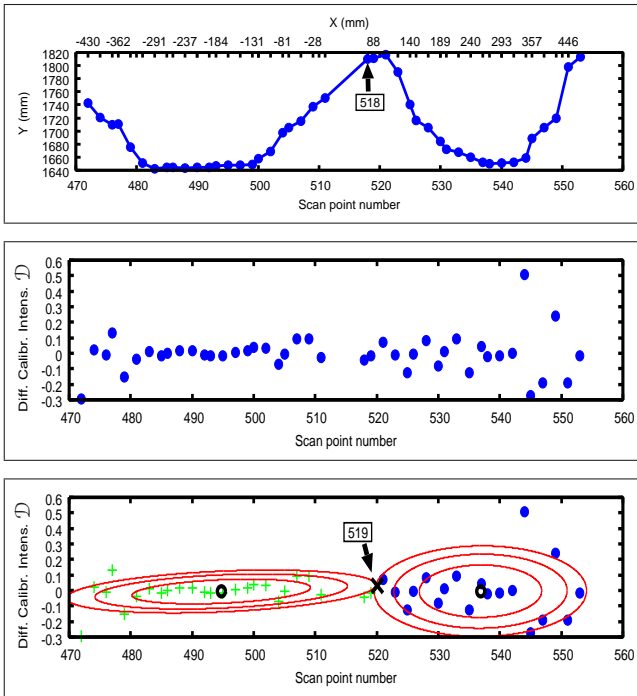For separation such person-merged segments, consider two different objects i and j which intensity difference

Fig. 4: Segment separation: (a) scan data in Cartesian coordinates, (b) $\mathcal{D}$ data, (c) EM for segment separation, "O" estimated mean of each Gaussian, "X" breakpoint.

$\mathcal{D}$ is normally distributed, i.e., $\mathcal{D}_i \sim \mathcal{N}(\mu_{\mathcal{D}_i}, \sigma^2_{\mathcal{D}_i})$ and $\mathcal{D}_j \sim \mathcal{N}(\mu_{\mathcal{D}_j}, \sigma^2_{\mathcal{D}_j})$, with mean $\mu_{\mathcal{D}}$ and variance $\sigma^2_{\mathcal{D}}$. Consider also that both objects are in contact so that they form one segment of scan data. The intensity distribution of the combined objects is the *Gaussian Mixture* $\mathcal{M}$ of both individual intensity distributions:

$$\mathcal{M}(\mathbf{x}) = \omega_i P(\mathbf{x}|\boldsymbol{\theta}_i) + \omega_j P(\mathbf{x}|\boldsymbol{\theta}_j) \qquad (6)$$

with $\mathbf{x} \in \mathcal{D}_{ij}$ and P the probability density function and the mixture weights ω_i and ω_j. The task of separating merged segments can be considered as the problem of separating the combined intensity distribution $\mathcal{D}_{ij}$ for objects i and j which implies estimating the unknown parameters: $\boldsymbol{\theta}_i = \langle \mu_{\mathcal{D}_i}, \sigma^2_{\mathcal{D}_i} \rangle$, $\boldsymbol{\theta}_j = \langle \mu_{\mathcal{D}_j}, \sigma^2_{\mathcal{D}_j} \rangle$, with a known parameter $N = 2$ the number of objects that define the mixture. We use the *Expectation-Maximization* (EM) algorithm to estimate $\boldsymbol{\theta}_i$ and $\boldsymbol{\theta}_j$ and then we separate data into respective distributions $\mathcal{D}_i$ and $\mathcal{D}_j$. After separation of difference of intensity data into respective distributions, the breakpoint is defined as the average of the last point in $\mathcal{D}_i$ and the first point in $\mathcal{D}_j$.

In Fig. 4 we present separation of a long segment from two persons standing very closed (merged). To ease visualization in Fig. 4(a) we include segments' data in Cartesian coordinates (the scan point number axis is also included), the actual breakpoint (labeled manually) is indicated. In Fig. 4(b) we show the graph of differences of intensity ($\mathcal{D}$) for the merged segments, each segment has different uniformity: points on the left half of Fig. 4(b) are tighter (vertical distance between points) than those on the right. In Fig. 4(c) we use EM for separation with points separated into respective distributions, the estimated means and covariance ellipses (up to 3σ) and

the breakpoint are shown. This method works when there is a difference in intensity uniformity in the two segments, if the two distributions $\mathcal{D}_i$ and $\mathcal{D}_j$ are rather similar then separation is inaccurate.

Given our intuitive method for merged segment detection based the segment width w, size ratio ℓ and variance $\sigma^2_{\mathcal{D}}$ and the proposed method for segment separation, we formalize our merged segment detection and separation in Algorithm 1, considering also the case of multiple merged objects.

Algorithm 1 Intensity-based segment separation

1: **for** every non-candidate segment S_i **do**
2:      **if** $\ell_i < \ell_{\max}$ and $w_i > w_{\max}$ **then** /*is not a person*/
3:          **if** $\sigma^2_{\mathcal{D}_i} > \sigma^2_{\mathcal{D}_{\min}}$ **then** /*intensity is not uniform*/
4:              Separate S_i into $S_{i,1}$ and $S_{i,2}$ using EM
5:              Feature extraction & classification for $S_{i,1}$, $S_{i,2}$
6:              Replace S_i by $S_{i,1}$ and $S_{i,2}$ in the list of segments /*$S_{i,1}$ and $S_{i,2}$ are also subject to merged segments check*/
7:          **end if**
8:      **end if**
9: **end for**

IV. EXPERIMENTAL RESULTS

We use four Hokuyo *URG-04LX* range scanner sensors, each operating at $10Hz$ covering distances up to $5.6m$, angular range of 240° and angular resolution of 0.36^o. This sensor uses a near-infrared (NIR) solid-state laser with $785nm$ wavelength. For data processing and robot control we use a notebook computer with an Intel Core 2 Duo processor at $1.83GHz$, $2GB$ of RAM, running Linux (kernel 2.6.35) as operating system. The processing time from sensor fusion to people detection was in average $52ms$, fast enough given the sensor's scanning speed of $100ms$.

Normally, *URG-04LX*'s range data consists in 682 points circularly ordered from right to left and with an angular resolution of 0.36^o. However, in order to obtain range and intensity simultaneously from the sensor, the number of scan points decreases to one half (341 points) and the angular resolution becomes 0.72^o. LRF data was obtained using this configuration. Data was obtained after warming up the sensors for about $60mins$ to avoid range and intensity drifting due to changes in internal sensor temperature [20], in this work we do not attempt temperature calibration of laser intensity.

A. Multi-layered People Detection

We obtained experimental data from 3 different environments and conditions for a robot and a group of people:

- A cluttered area ("Cluttered")
- Several people around the robot ("Crowded")
- Robot moving with people narrow hallways ("Mobile")

We present pictures of the different scenarios in the left column of Fig. 5, the robot position is marked with an arrow. The "Cluttered" test (Fig. 5(a)) consists in a wide area with some cluttering (chairs, dust bins, panels) causing

occlusions in the bottom layer, here two persons moved around the robot, moving in front and behind the obstacles. The "Crowded" test (Fig. 5(b)) is a wide environment with no cluttering but includes 12 people of diverse sizes and clothes colors moving around the robot. Finally the "Mobile" test (Fig. 5(c)) consists in long and narrow passages with cluttering (shoe-racks, umbrella stands, stairways, etc.), where the robot moved inside a group of three persons (operated by remote control), this case presented also occlusions and frequent merging of segments between people and walls. In the right column of Fig. 5 we include snapshots of our detection system (darker points correspond to top layer). In every figure detected persons are labeled as P_i and marked with a cylinder.

We present the range-based detection rates—without intensity features—for every case in the upper part of Table I (row labeled "without"), scan segments were manually labeled into person or not-person to establish the ground truth. The "Cluttered" test consisted in 473 multi-layer observations (parallel scans) and a total of 18172 segments, the true detection rate was 89.2%, false positive rate was 7.5% mostly due to misclassification of some columns, poster panels and curtains in the environment, and a false negative rate of 3.3% due to people walking behind panels and not being detected immediately after reappearing. The "Crowded" test consisted in 164 observations (6351 segments) for a true detection rate of 85.4%, complete occlusions (people walking behind people and very close) is largely responsible for the 11.6% false negative rate. Finally the "Mobile" test had 1238 observations (27662 segments) for a detection rate of 77.4%,
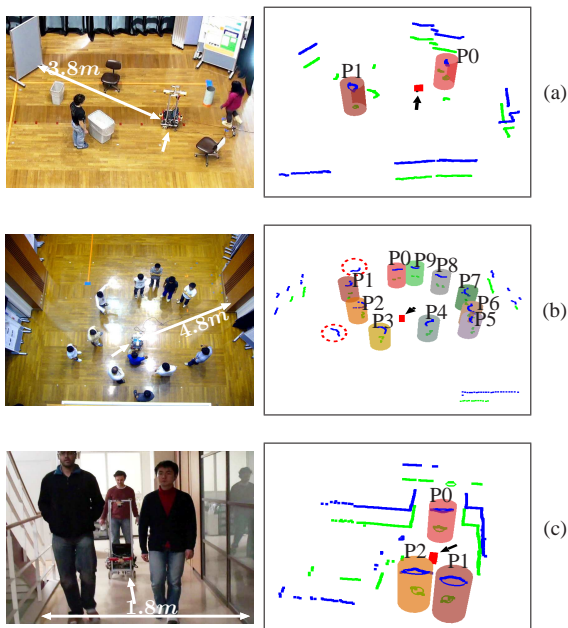
several environment objects (particularly block windows) were misclassified as people (9.4% false positive rate) and people walking close to the walls largely accounts for the 13.2% false negative rate.

TABLE I: Multi-Layer detection rates

	Test	True Detection	False Positive	False Negative
Without	Cluttered	89.2%	7.5%	3.3%
	Crowded	85.4%	3.0%	11.6%
	Mobile	77.4%	9.4%	13.2%
With	Cluttered	**92.6%**	4.2%	3.2%
	Crowded	**90.7%**	2.6%	6.7%
	Mobile	**88.2%**	6.7%	5.1%

B. People Detection Using Intensity

Using same scan data from the previous test scenarios, we repeated the detection evaluation but this time using laser reflection intensity (features $\sigma_{\mathcal{I}}^2$ and $\sigma_{\mathcal{D}}^2$, and segment separation). Detection results for every case are summarized in the lower part of Table I (row labeled "with"). In the "Cluttered" test the number of false negatives did not changed much due to the same problem explained above, the true detection rate increased 3.4%. In the other tests, higher increase in the true detection rate was achieved: 5.3% for the "Crowded" test and 10.8% for the "Mobile" test. Although features $\sigma_{\mathcal{I}}^2$ and $\sigma_{\mathcal{D}}^2$ contributed to increase the detection rate, segment separation contributed importantly in reducing the false negative rates (misdetections).

C. Single-layered People Detection

To compare results of our multi-layered people detection system (with and without laser intensity), we include the detection results of a single-layered detection system for the four test environments. Using log data from the same experiments, we selected all candidate segments detected by top layer strong classifiers $\mathcal{H}_{\text{top}}$ and $\mathcal{H}_{\text{top}}^+$ as valid persons.

TABLE II: Single-Layer detection rates

	Test	True Detection	False Positive	False Negative
Without	Cluttered	67.3%	21.2%	11.5%
	Crowded	76.7%	4.3%	19.0%
	Mobile	60.1%	19.7%	20.2%
With	Cluttered	**75.5%**	18.5%	6.0%
	Crowded	**86.3%**	4.5%	9.2%
	Mobile	**70.3%**	17.0%	12.7%

In Table II we report the single-layered detection results, without using laser intensity features in the upper part and using laser intensity in the bottom part. As presented, the true detection rates for all the experiments are by far lower to those of our multi-layered system, however using laser intensity improves the detection results in the single-layer system. False positives do not decrease much even by using laser intensity, due to misclassification in the single-layered system; the multi-layered system achieves better detection rates with smaller misclassification rates.

Fig. 5: Scenarios and results of three different experiments: "Cluttered" test (a) detected persons are $P0$ and $P1$; "Crowded" test (b) 10 out of 12 persons detected $P0$ to $P9$ (missing persons marked with circles); "Mobile" test (c) detected people are $P0$, $P1$ and $P2$.

V. Conclusions and Future Works

People detection using multi-layered LRF sensors and laser reflection intensity was was covered in this work. AdaBoost was used to train a strong classifier to detect body parts, candidate segments are combined for people detection and position estimation. Two new features were introduced improving people detection: intensity variation and intensity uniformity. Laser reflection intensity was also introduced to solve the problem of separation of merged segments. By analyzing the intensity uniformity we separate two objects merged together. As laser intensity decays with range a calibration method was also introduced.

As future works, the possibility of person identification using laser reflection intensity will be studied, and Multiple hypothesis tracking (MHT) will also be considered for tracking. Other future steps of this research include robot navigation inside the people group with assignment of roles.

References

[1] A. Carballo, A. Ohya, and S. Yuta, "Fusion of double layered multiple laser range finders for people detection from a mobile robot," in *IEEE International Conference on Multisensor Fusion and Integration for Intelligent Systems (MFI)*, Seoul, Korea, August 2008, pp. 677–682.

[2] A. Fod, A. Howard, and M. J. Matarić, "Laser-based people tracking," in *IEEE International Conference on Robotics and Automation (ICRA)*, Washington D.C., May 2002, pp. 3024–3029.

[3] M. Montemerlo, S. Thrun, and W. Whittaker, "Conditional particle filters for simultaneous mobile robot localization and people-tracking," in *IEEE International Conference on Robotics and Automation (ICRA)*, Washington, D.C., May 2002, pp. 695–701.

[4] H. Zhao, Y. Chen, X. Shao, K. Katabira, and R. Shibasaki, "Monitoring a populated environment using single-row laser range scanners from a mobile platform," in *IEEE International Conference on Robotics and Automation (ICRA)*, Roma, Italy, April 2007, pp. 4739–4745.

[5] K. O. Arras, Ó. Martínez Mozos, and W. Burgard, "Using boosted features for the detection of people in 2d range data," in *IEEE International Conference on Robotics and Automation (ICRA)*, Roma, Italy, April 2007, pp. 3402–3407.

[6] M. Hashimoto, K. Takahashi, and Y. Matsui, "Moving-object tracking with multi-laser range sensors for mobile robot navigation," in *IEEE International Conference on Robotics and Biomimetics (ROBIO)*, Sanya, China, December 2007, pp. 399–404.

[7] Ó. Martínez Mozos, R. Kurazume, and T. Hasegawa, "Multi-layer people detection using 2d range data," *International Journal of Social Robotics*, vol. 2, no. 1, pp. 31–40, 2010.

[8] R. E. Schapire and Y. Singer, "Improved Boosting Algorithms Using Confidence-rated Predictions," *Machine learning*, vol. 37, no. 3, pp. 297–336, 1999.

[9] Z. Zivkovic and B. Kröse, "Part based people detection using 2d range data and images," in *IEEE International*

Conference on Intelligent Robots and Systems (IROS), San Diego CA, October 2007, pp. 214–219.

[10] M. Mucientes and W. Burgard, "Multiple hypothesis tracking of clusters of people," in *IEEE/RSJ International Conference on Intelligent Robots and Systems (IROS)*, Beijing, China, October 2006, pp. 692–697.

[11] K. O. Arras, S. Grzonka, M. Luber, and W. Burgard, "Efficient people tracking in laser range data using a multi-hypothesis leg-tracker with adaptive occlusion probabilities," in *IEEE International Conference on Robotics and Automation (ICRA)*, Pasadena CA, May 2008, pp. 1710–1715.

[12] M. Luber, G. D. Tipaldi, and K. O. Arras, "Spatially grounded multi-hypothesis tracking of people," in *Proceedings of the IEEE ICRA 2009 Workshop on People Detection and Tracking*, K. O. Arras and Ó. Martínez Mozos, Eds., Kobe, Japan, May 2009, pp. 73–80.

[13] K. Klasing, D. Wollherr, and M. Buss, "Realtime segmentation of range data using continuous nearest neighbors," in *IEEE International Conference on Robotics and Automation (ICRA)*, Kobe, Japan, May 2009, pp. 4287–4292.

[14] J. Hancock, "Laser intensity-based obstacle detection and tracking," Ph.D. dissertation, Robotics Institute, Carnegie Mellon University, Pittsburgh, PA, January 1999.

[15] H. Surmann, A. Nüchter, and J. Hertzberg, "An autonomous mobile robot with a 3d laser range finder for 3d exploration and digitalization of indoor environments," *Robotics and Autonomous Systems*, vol. 45, no. 3-4, pp. 181–198, 2003.

[16] A. Nüchter, H. Surmann, and J. Hertzberg, "Automatic classification of objects in 3d laser range scans," in *8th Conference on Intelligent Autonomous Systems (IAS)*, Amsterdam, Netherlands, March 2005, pp. 963–970.

[17] M. Montemerlo, J. Becker, S. Bhat, H. Dahlkamp, D. Dolgov, S. Ettinger, D. Haehnel, T. Hilden, G. Hoffmann, B. Huhnke, D. Johnston, S. Klumpp, D. Langer, A. Levandowski, J. Levinson, J. Marcil, D. Orenstein, J. Paefgen, I. Penny, A. Petrovskaya, M. Pflueger, G. Stanek, D. Stavens, A. Vogt, and S. Thrun, "Junior: The Stanford Entry in the Urban Challenge," *Journal of Field Robotics*, vol. 25, no. 9, 2008.

[18] H. Kawata, K. Miyachi, Y. Hara, A. Ohya, and S. Yuta, "A method for estimation of lightness of objects with intensity data from sokuiki sensor," in *IEEE International Conference on Multisensor Fusion and Integration for Intelligent Systems (MFI)*, Seoul, Korea, August 2008, pp. 661–664.

[19] D. Jukić, G. Kralik, and R. Scitovski, "Least-squares fitting gompertz curve," *Journal of Computational and Applied Mathematics*, vol. 169, pp. 359–375, 2004.

[20] J. Pascoal, L. Marques, and A. T. de Almeida, "Assessment of laser range finders in risky environments," in *IEEE/RSJ International Conference on Intelligent Robots and Systems (IROS)*, Nice, France, September 2008, pp. 3533–3538.